0337

Referenceless Nyquist Ghost Correction Outperforms Standard Navigator Based Method for DT-CMR

Zimu Huo[1,2], Ke Wen[1], Yaqing Luo[1], Pedro F Ferreira[1], Radhouene Neji[3,4], Dudley Pennell[1], Andrew D Scott[1], and Sonia Nielles-Vallespin[1]
[1]CMR Unit, Royal Brompton Hospital and NHLI, Imperial college London, London, United Kingdom, [2]Department of Bioengineering, Imperial College London, London, United Kingdom, [3]School of Biomedical Engineering and Imaging Sciences, King's College London, London, United Kingdom, [4]MR Research Collaborations, Siemens Healthcare Limited, Frimley, United Kingdom

Synopsis

Keywords: Myocardium, Diffusion Tensor Imaging

Nyquist ghosting is a common artefact in echo planar imaging (EPI), typically corrected using separately acquired reference data. Here we demonstrate that reference free Nyquist ghost correction algorithms based on entropy and Ghost/Object ratio minimization can outperform navigator based methods and improve imaging efficiency for in vivo diffusion tensor cardiovascular magnetic resonance.

Introduction

Echo planar imaging (EPI) is subject to Nyquist ghosting due to misalignment of the forward and reverse lines of k-space. These artefacts are commonly corrected using the well-established three line navigators[1] methods. Alternatively, reference-free methods have demonstrated Nyquist ghost correction without the need to acquire additional reference scans in the breast and brain[2-3]. Diffusion tensor cardiovascular magnetic resonance (DT-CMR) typically relies on single shot EPI acquisitions with separately acquired phase correction navigators, which reduce the efficiency of this already time consuming mehtod[4]. This work aims to investigate and compare the performance of a standard navigator-based method, to referenceless entropy based[2], and the Ghost/Object minimization[3] method in application to DT-CMR.

Method

Acquisition

DT-CMR systolic, breath hold, motion compensated Spin Echo[5] (SE) and STEAM[4] EPI data were acquired in the mid-ventricular short axis from 16 healthy volunteers. The "b0" image is acquired with b ~ 30 $s \cdot mm^{-2}$ followed by 6 diffusion encoding directions with 2 repetitions at b = 150 $s \cdot mm^{-2}$ and 8 to 10 repetitions with 450 $s \cdot mm^{-2}$ and 600 $s \cdot mm^{-2}$ for SE and STEAM respectively. The imaging parameters are as follow: TE = 62 ms and 22 ms for SE and STEAM respectively, field of view 360 by 135 mm^2, TR = 2 cardiac cycles, 2442 Hz/pixel bandwidth, 2.8 by 2.8 mm^2 or 1.4 by 1.4 mm^2 with zero padding, GRAPPA x2, and no partial Fourier used. The field of view was reduced in the phase encode direction by making the 1st (and 2nd for STEAM) RF pulse slice selective in the phase encode direction.

Reconstruction

The raw data were reconstructed offline using 4 methods 1) uncorrected, 2) navigator based ghost correction 3) entropy based ghost correction 4) Ghost/Object minimization.
Method 1: GRAPPA[6] kernels were trained on the ghosted reference data and then applied on the aliased dataset.
Method 2: A linear fit was first performed on the savgol filtered (order 4) phase difference obtained from the navigators in the hybrid space (1D inverse Fourier transform along frequency encode direction) to obtain the phase correction offset and slope. This phase shift is then applied to the data followed by an standard GRAPPA in plane reconstruction.
Method 3: Brute force search was used find the phase correction offset and slope corresponding to the minimum image entropy. This phase correction was applied before GRAPPA reconstruction as in 2.
Method 4: Reconstruction as for method 3, but the cost function is replaced with f,

$$f^{-1} = \sum_{x,y} F_{med2D} \frac{|I_{x,y}|}{|I'_{x,y}|}$$

where F is the 2D median filter, I is the measured image in image space(x, y), and I' is the copy of I shifted by half field of view in the phase encoding direction.
The phase errors between even and odd lines (after FFT along FE) were modelled with a linear fit for all methods. The Nyquist Ghost intensity is measured using the relative intensity outside the spin or stimulated echo field of view as shown in figure 1. DT-CMR data is processed using in-house MATLAB (Mathworks, Natick, Massachusetts, USA) software.

Result

Examples of ghost correction for all 4 methods are shown in Figure 2. The average ghost intensity for the entropy(0.0790±0.0303) and Ghost/Object (0.0797±0.0305) methods are significantly lower ($p<0.005$) than that of the navigator based method (0.1210±0.0439) as shown in figure 3. The performance is also consistent across all diffusion weightings and sequence types. Examples of the DT-CMR maps are shown in figure 4 for all correction methods, and the averaged DT-CMR measures are compared in figure 5.

Discussion

Correction methods show reduction in ghosting over the uncorrected image set, particularly the referenceless based corrections. As for the DT-CMR maps in figure 5, the increased FA and reduced MD using the referenceless methods are consistent with an increase in the SNR of the diiffusion weighted images[7-8].
Referenceless methods such as the entropy and Ghost/Object minimisation are robust and efficient, because they do not require additional reference scans, which saves acquisition time. The scan time reduction provided by the referenceless methods allows at least 8 additional images to be acquired in the same amount of time in our clinical research DT-CMR protocol. However, when using the entropy based method, care must be taken when setting the search range of the phase offset parameter, as the result may deviate from the true ghost correction parameters if the range is too large and the algorithm will try to enhance the ghost and remove the parent object. As a result, the cost function for the Ghost/Object method may be preferred for a more stable outcome when the reduced phase field of view method can be used.
In conlusion, although the computational cost is higher for the referenceless methods, the image quality improvement and acquisition time saving makes these methods valuable additions to the DT-CMR image reconstruction pipeline, paving the way for clinically feasible in vivo DT-CMR.

Acknowledgements

The authors would like to thank the research radiographers Raj Soundarajan and Gover Simon for their immense support and guidance in data acquistion.

References

1. Heid, O. Method for the phase correction of nuclear magnetic resonance signals. US Patent 6,043,651. 2000.

2. Clare, S. Iterative Nyquist ghost correction for single and multi-shot EPI using an entropy measure. In Proceedings of ISMRM. 2003;p.1041.

3. McKay JA, Moeller S, Zhang L, Auerbach EJ, Nelson MT, Bolan PJ. Nyquist ghost correction of breast diffusion weighted imaging using referenceless methods. Magn Reson Med. 2019;81:2624–2631. https://doi.org/10.1002/mrm.27563

4. Nielles-Vallespin S, Mekkaoui C, Gatehouse P, Reese TG, Keegan J, Ferreira PF, Collins S, Speier P, Feiweier T, de Silva R, Jackowski MP, Pennell DJ, Sosnovik DE, Firmin D. In vivo diffusion tensor MRI of the human heart: reproducibility of breath-hold and navigator-based approaches. Magn Reson Med. 2013 Aug;70(2):454-65. doi: 10.1002/mrm.24488. Epub 2012 Sep 21. Erratum in: Magn Reson Med. 2014 Aug;72(2):599. PMID: 23001828; PMCID: PMC3864770.

5. Welsh CL, DiBella EV, Hsu EW. Higher-Order Motion-Compensation for In Vivo Cardiac Diffusion Tensor Imaging in Rats. IEEE Trans Med Imaging. 2015 Sep;34(9):1843-53. doi: 10.1109/TMI.2015.2411571. Epub 2015 Mar 9. PMID: 25775486; PMCID: PMC4560625.

6. Griswold MA, Jakob PM, Heidemann RM, Nittka M, Jellus V, Wang J, Kiefer B, Haase A. Generalized autocalibrating partially parallel acquisitions (GRAPPA). Magn Reson Med. 2002 Jun;47(6):1202-10. doi: 10.1002/mrm.10171. PMID: 12111967.

7. Scott, A.D., Nielles-Vallespin, S., Ferreira, P.F. et al. An in-vivo comparison of stimulated-echo and motion compensated spin-echo sequences for 3 T diffusion tensor cardiovascular magnetic resonance at multiple cardiac phases. J Cardiovasc Magn Reson 20, 1 (2018). https://doi.org/10.1186/s12968-017-0425-8

8. Jones DK, Basser PJ. "Squashing peanuts and smashing pumpkins": how noise distorts diffusion-weighted MR data. Magn Reson Med. 2004 Nov;52(5):979-93. doi: 10.1002/mrm.20283. PMID: 15508154.

Figures

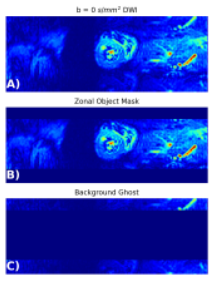

Figure 1. Measurement of the Nyquist ghosts. This example A) highlights the Nyquist ghost for uncorrected b0 image.The image B) shows the zonal mask which separates the object and ghost. The image C) shows the residual ghost outside reduced field of view. The level of ghosting is measured by the sum of the magnitude image outside the reduced field of view.

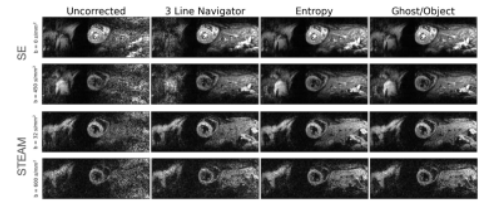

Figure 2. Single slice of mid short axis view systole cardiovascular DT-CMR. In this example, the referenceless methods show less ghosting artefact than the standard navigator method for both sequences and diffusion weightings.

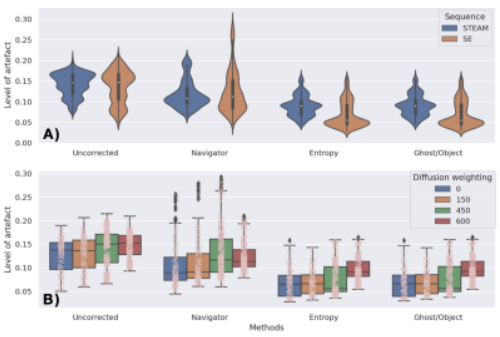

Figure 3. Residual ghost intensity across correction methods shown by sequence type (A) and diffusion weighting (B). The white dot in the middle of the violin plot indicates the median ghost level and the black bar in the center of violin represents the interquartile range. The black dots in the box plot correspond to outliers, and white pink circles correspond to other samples.

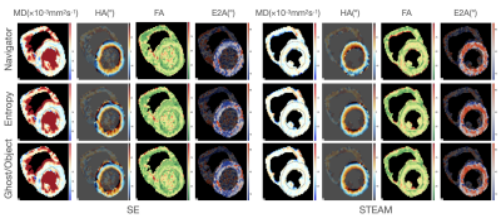

Figure 4. Example of DT-CMR maps from one healthy subject for SE and STEAM with different correction methods, including mean diffusivity (MD), helix angle (HA), fractional anisotropy (FA), and absolute second eigenvector angle (E2A). Despite the potential reduction in acquisition time, the referenceless method appear similiar quality to the navigator based correction.

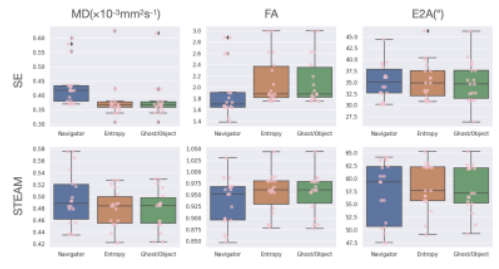

Figure 5. DT-CMR results for all subjects: mean left ventrical mean diffusivity (MD), mean fractional anisotropy (FA), and the median of the absolute value of the second eigenvector angle (E2A). The referenceless methods result in a reduction in MD and an increase in FA particularly for the SE data.

Proc. Intl. Soc. Mag. Reson. Med. 31 (2023)
0337